



HAL
open science

A tensorial description of stresses in triphasic granular materials with interfaces

R. Wan, Jérôme Duriez, F. Darve

► **To cite this version:**

R. Wan, Jérôme Duriez, F. Darve. A tensorial description of stresses in triphasic granular materials with interfaces. *Geomechanics for Energy and the Environment*, 2015, 4, pp.73 - 87. 10.1016/j.gete.2015.11.004 . hal-01865375

HAL Id: hal-01865375

<https://hal.science/hal-01865375>

Submitted on 31 Aug 2018

HAL is a multi-disciplinary open access archive for the deposit and dissemination of scientific research documents, whether they are published or not. The documents may come from teaching and research institutions in France or abroad, or from public or private research centers.

L'archive ouverte pluridisciplinaire **HAL**, est destinée au dépôt et à la diffusion de documents scientifiques de niveau recherche, publiés ou non, émanant des établissements d'enseignement et de recherche français ou étrangers, des laboratoires publics ou privés.

A tensorial description of stresses in triphasic granular materials with interfaces

R. Wan^a, J. Duriez^a, F. Darve^b

^a*Department of Civil Engineering, University of Calgary, Calgary, AB, T2N 1N4, Canada*

^b*Univ. Grenoble Alpes, 3SR, F-38000 Grenoble, France
CNRS, 3SR, F-38000 Grenoble, France*

Abstract

The description of stress transmission in an unsaturated granular material in the low water saturation range (pendular regime) is studied within the micromechanics of a three-phase medium. Considering an REV (Representative Element Volume) comprised of solid grains and isolated inviscid water menisci whose statistical distributions are known, micro- and macro-relationships can be derived using a volume-averaging of stress for each one of the phases in a manner analogous to the derivation of Love-Weber equation defining stress in a dry granular medium. The main difference with respect to previous works in the literature lies in the homogenization technique whereby singular surfaces such as an air-water interface exhibiting surface tension are treated as an additional phase for which a so-called membrane stress is defined. Well-known contractile skin effects and the anisotropy of capillary stresses in unsaturated soils can be formally identified in the proposed tensorial expression that encompasses the statistics of not only grain contact normals, but also that of menisci spatial orientations and their surfaces, including water saturation. Solid grains are considered strictly incompressible with water being also an incompressible and inviscid liquid. An effective stress tensor that controls the strength of unsaturated granular media is hence proposed and verified based on discrete element modelling (DEM) numerical simulations of triaxial compression and simple shear tests on pendular-state granular soils at different confining pressures and matric suctions. The non-sphericity of the so-called capillary stress is also numerically demonstrated.

Keywords: pendular regime, effective stress, interfacial tension, wetting-drying, suction

1. Introduction

The derivation of a tensorial stress field in a continuum representation of an unsaturated particulate medium like a geomaterial is well studied in the literature; see [33, 13, 26], among others. While microstructural aspects have lately been subject of considerable interest, a largely theoretical issue that is often evoked is the definition of a single-valued effective stress [8, 32, 42] that controls both deformation and strength in such unsaturated media, and which replaces the celebrated Terzaghi's effective stress in the fully saturated case. This question takes on a more practical importance in geotechnical/geo-environmental engineering, motivated by the shrinkage, swelling, yielding and collapse of unsaturated soils at low water saturation upon drying and wetting cycles associated with weather change or the natural hydrologic cycle, e.g. [29].

Herein, we are particularly interested in the pendular regime where water saturation is low and the water phase is held in between the interstices of the granular material (soil) in the form of isolated menisci [4, 38]. In this case, the solid phase is comprised of a grain skeleton whose interstices are occupied by air as a continuous phase and water as a discontinuous phase, with interfaces that separate the various phases. Hence, the mechanics of the unsaturated granular system is invariably governed by the different phases whose individual behaviours are well defined, and also interfaces that are endowed with thermodynamics properties [20, 30]. Problems associated with unsaturated soil mechanics and related

24 fields specifically involve fluid flow, stress, thermal, chemical and defor-
 25 mation phenomena which are essentially coupled. Here in this paper, we
 26 are specifically interested in stress phenomena that encompass classical
 27 geotechnical problems under unsaturated conditions where the question
 28 of stress transport and strength are of critical concern, but yet difficult to
 29 discern.

30 Historically, Bishop's stress [5] as an extension to Terzaghi's effective
 31 stress has been a commonly used stress in unsaturated soils according to
 32 the following tensorial form:

$$\begin{aligned}\sigma'_{ij} &= \sigma_{ij} - (1 - \chi)u_a\delta_{ij} - \chi u_w \delta_{ij} \\ &= \bar{\sigma}_{ij} + \chi(u_a - u_w) \delta_{ij}\end{aligned}\tag{1}$$

33 where σ'_{ij} is the Bishop's stress tensor, $\bar{\sigma}_{ij} = (\sigma_{ij} - u_a \delta_{ij})$ is the so-called
 34 net stress, χ is generally assumed to be a function of degree of saturation
 35 and is zero for dry soil and unity for saturated soil, and the term $(u_a -$
 36 $u_w)$ represents matric suction s . Herein, soil mechanics sign convention
 37 is adopted throughout the paper, i.e. compressive stresses and strains are
 38 positive.

39 Over the years, Bishop's equation has been the subject of controversy
 40 [23] and even Bishop and Blight [6] admitted that there are uncertainties
 41 over the definition of parameter χ , although much later on, Gray and Has-
 42 sanizadeh [18] proved that Bishop's stress is thermodynamically consis-
 43 tent when χ is associated with degree of saturation. Moreover, Blight [7]

44 argued that the value of χ depends on stress and strain levels; whereas
45 nowadays, Wan et al. [44], Duriez and Wan [15] have established its link
46 to fabric and meniscus spatial distribution which furthermore destroys the
47 isotropic character of the matric suction in the original Bishop's equation.

48 Uncertainties in finding a single-valued stress variable prompted the
49 idea that the behaviour of unsaturated soils should be governed inde-
50 pendently by two variables: the net stress $(\sigma - u_a)$ and matric suction
51 $(u_a - u_w)$. Fredlund and Morgenstern [17] went on further to suggest
52 that any two of the stress state variables $\bar{\sigma} = (\sigma - u_a)$, $\sigma' = (\sigma - u_w)$,
53 and $s = (u_a - u_w)$ could be employed. Furthermore, Houlsby [21] devel-
54 oped the concept of power input into unsaturated soils, and hence intro-
55 duced the notion of work conjugate stress and strain increment variables
56 for constitutive modelling, but without including the energy of the inter-
57 faces. The idea of average soil skeleton thus emerged.

58 More recent studies have focused on the understanding of unsaturated
59 soil behaviour through continuum approaches such as mixture theory [9,
60 40]. As such, there has been a number of stress measures defined for unsat-
61 urated granular media and which have made their way to soil mechanics
62 and reservoir engineering. These are the total stress, the skeleton stress
63 [19], the net stress [1], the generalized Bishop [5] stress, and the Skemp-
64 ton [41] stress. Approaches that are based on total stresses have even been
65 proposed for triphasic media, but then, they would necessitate the writ-
66 ing of equations of equilibrium and associated boundary conditions for

67 each phase; see [30] which circumvents this latter requirement. Given
68 the overall progress of granular mechanics in the past several decades,
69 renewed efforts to address the above theoretical and practical questions
70 seem appropriate. With this motivation, this paper provides a systematic
71 microstructural study in which a tensorial stress expression is derived for
72 a triphasic material composed of air, water and solid, with the water phase
73 being discontinuously distributed as isolated menisci (liquid bridges) be-
74 tween particles that can be either in contact or not. As for the solid phase,
75 we consider distinct idealized particles of spherical shape. Additionally,
76 the air-water interface along with a jump condition at the common line is
77 included in the derivation as a fourth phase .

78 The proposed method uses a volume averaging of stress for each one of
79 the phases in a manner analogous to the derivation of Love-Weber equa-
80 tion [28, 45] defining stress in a dry granular medium to arrive at a tenso-
81 rial expression for stress that encompasses the statistics of not only grain
82 contact normals, but also that of menisci spatial orientations and menisci
83 surfaces, including water saturation. More importantly, an effective stress
84 tensor can be recognized as the difference between the total stress tensor
85 and so-called capillary stresses that include contributions from suction,
86 surface tension, and air-water interface associated tensors. As new re-
87 sults, we identify menisci induced effects within the unsaturated granular
88 medium through:

- 89 1. a surface based fabric tensor of menisci scaled by the matric suction,

- 90 2. lineal surface tension force contributions along wetted grain con-
 91 tours, and
- 92 3. a spatial distribution of surface tension force field (tensorial) within
 93 air-water interfaces.

94 The validity of the proposed effective stress equation, including other
 95 features such as the non-sphericity of the capillary stresses are verified via
 96 discrete element modelling (DEM) simulations.

97 **2. Micromechanics of a triphasic medium**

98 *2.1. Preliminaries*

The notion of stress within a continuous body goes as far back to Cauchy who introduced this abstract conceptual scheme where the mutual action of two bodies in contact, or two parts of the same body separated by an imaginary surface is contemplated [28]. This powerful conceptual idea can be extended to the definition of a stress tensor under quasi-static conditions for a heterogeneous body consisting of discrete particles of volume V_p . These are considered rigid, endowed with stress σ^p , and interact through contact points c with pairwise interparticle force \mathbf{f}^p in a granular assembly of volume V . Thus, the celebrated Love-Weber formula gives:

$$\sigma = \frac{1}{V} \sum_p \int_{\partial V_p} (\sigma^p \cdot \mathbf{n}) \otimes \mathbf{x}^p dS \quad (2a)$$

$$= \frac{1}{V} \sum_p \sum_c \mathbf{f}^p \otimes \mathbf{x}^p \quad (2b)$$

99 where $(\sigma^p \cdot \mathbf{n})$ is the traction vector on the particle p with outward normal
 100 \mathbf{n} , and the vector \mathbf{x}^p represents the spatial position of applied traction with
 101 respect to an arbitrary origin.

102 When sweeping over all contacts for every particle in volume V and
 103 by expressing the position vector \mathbf{x}^p as a function of the particle's centroid
 104 and radius vector, we get the classic expression given by:

$$\sigma = \frac{1}{V} \sum_{\alpha\beta} \mathbf{f}^{\alpha\beta} \otimes \boldsymbol{\ell}^{\alpha\beta} \quad (3)$$

105 where the summation is carried out over distinct pairs of particles $\alpha\beta$
 106 in V , $\mathbf{f}^{\alpha\beta}$ and $\boldsymbol{\ell}^{\alpha\beta}$ denote, respectively, the pairwise interaction force and
 107 branch vector giving distance of separation.

108 Equation (3), derived with the assumption of a quasi-static medium in
 109 the absence of any body forces, serves as the basis for calculating volume-
 110 average stresses in heterogenous media. For the case where the discrete
 111 particles are embedded into a matrix which includes singular surfaces
 112 over which surface tension occurs, the integral term in Eq. (2a) has to
 113 be amended. This is because some components of the stress tensor suffer
 114 a discontinuity associated with surface tension, as will be seen next when
 115 calculating the volume-average stress in a triphasic medium.

116 2.2. Averaging process with stress discontinuities

117 Consider a representative element volume (REV) of volume V contain-
 118 ing a statistically significant number of particles and water menisci as il-
 119 lustrated in Fig. 1.

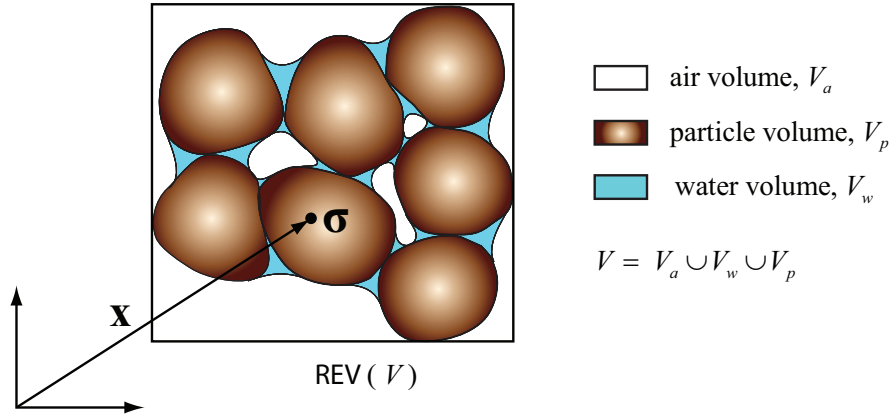


Figure 1: REV of pendular unsaturated medium

120 It also represents an averaging volume whose dimensions are large
 121 compared with the characteristic microscale (particle and water meniscus
 122 sizes) of the unsaturated granular material, but still arbitrarily small com-
 123 pared to the dimension of the soil domain. The solid particles are assumed
 124 to be strictly rigid interacting with incompressible air and inviscid water.

125 In practical terms, we wish to know what stress is generated within
 126 the REV when loads (mechanical or hydraulic) are applied on its external
 127 boundary. Since the actual stress σ_{ij} varies with position \mathbf{x} in the REV, the
 128 ‘bulk stress’ can be defined from an ensemble (volume) averaging. How-
 129 ever, a closer look at the REV reveals that we are faced with a three-phase
 130 system composed of solid (s), air (a) and water (w) separated by interfacial
 131 surfaces upon which a singularity in the stress distribution exists due to
 132 surface tension. A volume integral of the stress over such a region is then
 133 strictly speaking improper, and must be thus interpreted appropriately.

134 As such, the average stress Σ_{ij} is computed just as volume averages of
 135 stress in all phases concerned, including the interfaces, i.e.

$$\Sigma_{ij} = \frac{1}{V} \left\{ \int_{V^p} \sigma_{ij} dV + \int_{V^w} \sigma_{ij} dV + \int_{V^a} \sigma_{ij} dV + \int_{V^{int}} \sigma_{ij} dV \right\} \quad (4)$$

136 Herein, it is appropriate to regard the interface between air and water
 137 as a layer of small thickness ϵ , and to subsequently take the limit $\epsilon \rightarrow 0$.
 138 For a given point on the interface, if the local normal is denoted by unit
 139 normal \mathbf{n} , then the surface tension force field tensor can be written in the
 140 form $\gamma(\delta_{ij} - n_i n_j)$ where γ is the coefficient of surface tension. On the other
 141 hand, the stress components along directions in the tangent plane of the
 142 air-water interfacial surface are very large in the interface layer. Therefore,
 143 the correct stress integral properties can be obtained by taking the singular
 144 part of the stress tensor in the interface layer to be in the form $\sigma_{ij} = \gamma(\delta_{ij} -$
 145 $n_i n_j)/\epsilon$.

146 Noting the above, the contribution of the volume integral in Eq. (4)
 147 from the portion of the interfacial surface S^{aw} lying within the REV is then

$$\lim_{\epsilon \rightarrow 0} \int_{V^{int}} \sigma_{ij} dV = \int_{S^{aw}} \gamma(\delta_{ij} - n_i n_j) dS \quad (5)$$

148 The integral on the right hand side of Eq. (5) can be alternatively written
 149 as

$$\int_{S^{aw}} \gamma(\delta_{ij} - n_i n_j) dS = \int_{S^{aw}} \gamma n_i \text{div } \mathbf{n} x_j dS \quad (6)$$

150 by applying Stokes's theorem to the quantity $\epsilon_{kil} x_i n_l$, regarded as a vector
 151 with components given by the different values of k [36].

152 The term, $\text{div } \mathbf{n}$, is in fact the curvature of the interfacial surface contain-
 153 ing the local normal \mathbf{n} , and hence $(\gamma n_i \text{div } \mathbf{n})$, which is the normal curva-
 154 ture force per unit area, represents the jump in the normal stress across the
 155 air-water interface due to surface tension, i.e. $(u_a - u_w)n_i$.

156 Noting the above and considering the pressures of the water and air
 157 phases to be hydrostatic, the volume-average stress in Eq. (4) can be re-
 158 written as:

$$\begin{aligned} \Sigma_{ij} = & \frac{1}{V} \sum_p \int_{V^p} \sigma_{ij} dV + \frac{1}{V} \int_{V^w} u_w \delta_{ij} dV + \frac{1}{V} \int_{V^a} u_a \delta_{ij} dV \\ & + \frac{1}{V} \sum_l \int_{S^{aw}} \gamma n_i \text{div } \mathbf{n} x_j dS \end{aligned} \quad (7)$$

159 where p and l are the number of particles and liquid bridges respectively,
 160 V^a and V^w are the volume occupied by air and water phases respectively,
 161 while u_a and u_w are the air and water pressures respectively.

162 Applying the divergence theorem to the volume integral concerning
 163 each particle in Eq. (7) leads to a surface integral just like in the opening
 164 Eq. (2a), except that the tractions exerted on the particle's surface with
 165 outward normal \mathbf{n} have now various origins. For instance, we will find
 166 contributions from pair-wise particle contact forces due to external load-
 167 ing, as well as actions of air and water pressures on dry (∂V_p^a) and wetted
 168 surfaces (∂V_p^w) respectively. Based on the above and noting Eq. (3), it

169 follows that

$$\begin{aligned} \Sigma_{ij} = & \frac{1}{V} \sum_{\alpha\beta} f_i^{\alpha\beta} \ell_j^{\alpha\beta} + \frac{u_w}{V} \sum_p \sum_l \int_{\partial V_p^w} n_i x_j dS + \frac{u_a}{V} \sum_p \int_{\partial V_p^a} n_i x_j dS \\ & + \frac{V_w}{V} u_w \delta_{ij} + \frac{V_a}{V} u_a \delta_{ij} + \frac{1}{V} \sum_l \int_{S_{awl}} \gamma n_i \operatorname{div} \mathbf{n} x_j dS \end{aligned} \quad (8)$$

170 where tractions acting on vanishing surface area over the contour ∂V_p of
 171 each particle p have been transformed into point (contact) forces $f_i^{\alpha\beta}$ be-
 172 tween pairs of particles $\alpha\beta$ joined by branch vector $\ell_j^{\alpha\beta}$.

173 By applying Stokes's theorem (see Appendix A), the interface integral
 174 can be re-written as

$$\frac{1}{V} \int_{S_{awl}} \gamma n_i \operatorname{div} \mathbf{n} x_j dS = -\frac{1}{V} \int_C T_i^{aw} x_j d\ell + \frac{1}{V} \int_S \frac{\partial \gamma}{\partial x_i} x_j dS \quad (9)$$

175 where $T_i^{aw} = \gamma t_i^{aw}$ refers to the surface tension force acting at the intersec-
 176 tion of the liquid bridge and the particle, i.e. the interface solid-air-water
 177 which creates the so-called contractile skin within the unsaturated granu-
 178 lar assembly.

179 Furthermore, noting that the surface area of a particle ∂V_p can be de-
 180 composed as a union of dry (air) surfaces ∂V_p^a and wetted surfaces over
 181 l liquid bridges, i.e. $\partial V_p = \partial V_p^a \cup \partial V_p^w$, the surface integral over the dry
 182 surfaces of a particle can be written as:

$$\int_{\partial V_p^a} n_i x_j dS = \int_{\partial V_p} n_i x_j dS - \sum_l \int_{\partial V_p^w} n_i x_j dS \quad (10)$$

183 Finally, in the absence of any gradient in surface tension force ($\partial \gamma / \partial x_i =$

184 0) we get:

$$\begin{aligned}
\Sigma_{ij} = & \frac{1}{V} \sum_{\alpha\beta} f_i^{\alpha\beta} \ell_j^{\alpha\beta} - \frac{(u_a - u_w)}{V} \sum_p \sum_l \int_{\partial V_p^w} n_i x_j dS \\
& + \frac{u_a}{V} \sum_p \int_{\partial V_p} n_i x_j dS + \frac{V_w}{V} u_w \delta_{ij} + \frac{V_a}{V} u_a \delta_{ij} \\
& - \frac{1}{V} \sum_p \sum_l \int_{\mathcal{C}} T_i^{aw} x_j d\ell
\end{aligned} \tag{11}$$

185 For a granular system consisting of particles of radius R_p , $x_i = R_p n_i$,
186 and noting $\phi = (V_a + V_w)/V$ and $S_r = V_w/(V_a + V_w)$, with $V = V_s +$
187 $V_w + V_a$, it follows after some manipulations that:

$$\left. \begin{aligned}
\Sigma_{ij} = & u_a \delta_{ij} + \frac{1}{V} \sum_{\alpha\beta} f_i^{\alpha\beta} \ell_j^{\alpha\beta} - \chi_{ij}(u_a - u_w) - B_{ij} \\
\text{where} \\
\chi_{ij} = & \frac{1}{V} \sum_p R_p \sum_l \int_{\partial V_p^w} n_i n_j dS + \phi S_r \delta_{ij} \\
B_{ij} = & \frac{1}{V} \sum_p R_p \sum_l \int_{\mathcal{C}} T_i^{aw} n_j d\ell
\end{aligned} \right\} \tag{12}$$

188 Equation (12) serves to establish an equivalence between a non homo-
189 geneous granular system with discontinuous air-water interfaces and an
190 equivalent homogeneous REV through the volume-average stress tensor
191 Σ . In fact, this relation bears some resemblance to Bishop's equation, but is
192 more complex in three major distinct aspects. First, the matric suction is no
193 longer an isotropic quantity, but is now governed by a Bishop-like param-
194 eter which is a tensor χ whose explicit form is known with dependences

195 on liquid bridge spatial distribution and degree of saturation, among oth-
 196 ers. Second, the influence of air-water interfacial tension on the granu-
 197 lar system behaviour is included through the new term B which involves
 198 integration of lineal surface tension forces over contours defined by the
 199 wetting of liquid bridges with the solid particles. Third, the expression
 200 makes a clear distinction between point forces at particle contacts and lin-
 201 eal forces arising from surface tension. In fact, these point forces are ex-
 202 erted at contacts of particle pairs $\alpha\beta$ to give rise to a so-called contact stress
 203 tensor σ^{cont} through the Love-Weber formula which is clearly recognizable
 204 in the first line of Eq. (12).

205 To make particular reference to the liquid bridge contributions to the
 206 total stress Σ , we conveniently define a so-called capillary stress tensor
 207 taken to be:

$$\sigma^{\text{cap}} = -(s\chi + B) = \Sigma - u_a \delta - \sigma^{\text{cont}} \quad (13)$$

208 Note that the “capillary stress” terminology, also used elsewhere in
 209 [39], is equivalent to the “suction stresses” alluded in Lu and Likos [29].

210 We will next endeavour to investigate the nature of capillary stresses
 211 σ^{cap} , as well as check whether the contact stress σ^{cont} can be regarded as an
 212 effective stress in Terzaghi’s sense. To achieve such a goal, we will adopt
 213 a DEM calculation approach to determine the water phase distribution
 214 within an unsaturated granular system so that Eq. (12), the central piece
 215 of this study, can be formally evaluated.

216 **3. Discrete modelling of a triphasic medium**

217 *3.1. The discrete model*

218 Generally speaking, numerical simulation of the mechanics of granular
219 material based on DEM consists of calculating the motion of a collection
220 of particles, the so-called discrete elements (DE), under the action of solely
221 point forces. Deformation of the granular ensemble then comes out of the
222 relative displacements of particles calculated following Newton's law of
223 motion under interaction forces and torques. The numerical simulations
224 can describe quite accurately salient behavioural features of real granular
225 materials, although particle shapes are idealized as disks or spheres and
226 the number of particles is relatively small compared to actual granular
227 masses.

228 For the discrete modelling of granular multiphase systems, liquid and
229 gas phases are included through the forces they impose on solid particles
230 as described in [35, 39, 31] for the unsaturated case, and in [11] for the
231 fully saturated case. It is worth noting that an embedded flow model [12]
232 is used in [11] to compute spatially varying water pressure field. How-
233 ever, if an homogeneous distribution of matric suction is assumed within
234 an unsaturated granular material, the water phase characteristics can be
235 readily computed. It is under such an assumption that the liquid bridge
236 distribution specific to the pendular regime can be determined by solv-
237 ing Laplace's equation [25] for all particle pairs. Following this approach,
238 Scholtès *et al.* [39] proposed a discrete model for unsaturated conditions,

239 within Yade open source code [43]. Therefore, the characteristics of liq-
 240 uid menisci being determined from Laplace’s equation for a zero contact
 241 angle, so-called capillary forces due to the water and air phases can be
 242 readily determined from the radius R of the particle, surface tension γ ,
 243 matric suction s , and filling angle α (Fig. 2), i.e.

$$\mathbf{f}^{\text{cap}} = \pi R \sin^2 \alpha (2\gamma + R s) \mathbf{x} \quad (14)$$

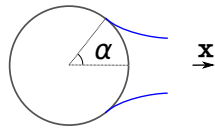


Figure 2: Liquid bridge geometry

244

245 Other discrete models for unsaturated granular materials differ mainly
 246 in the way the capillary force is computed, using often approximations
 247 based on assumptions made for the liquid volume [35, 31].

248 In this study, we use the discrete model proposed by Scholtès et al. [39]
 249 which is already implemented in the open source computer code YADE.

250 In addition to the capillary forces, contact interaction forces are computed
 251 from three basic numerical parameters and particles relative displacements.
 252 Classically, the contact behavior is elastic in the normal direction (tensile
 253 states being ruled out), and elastic-plastic in the tangential direction. Two
 254 first parameters, namely Y and P , refer to the normal and tangential con-

255 tact stiffnesses k_n, k_t for an interaction between particles A and B :

$$k_n = \frac{2Y R_A R_B}{R_A + R_B} \quad (15)$$

$$k_t = P k_n$$

256 Expressing k_n and k_t according to the particles radii R_A and R_B leads to a
 257 size independent behavior of the model in dry conditions. The third con-
 258 tact parameter is the local contact friction angle φ that restricts the tangen-
 259 tial force: $\|\vec{F}_t\| \leq F_n \tan(\varphi)$. A fourth numerical parameter enters as the
 260 particle size as discussed in Duriez and Wan [16] where the capillary force
 261 computations between contacting and distant particles make the response
 262 of the unsaturated granular system particle size dependent.

263 We herein choose a granular ensemble with a uniform particle size dis-
 264 tribution whose characteristics appear in Table 1 with other model param-
 265 eters.

Y (MPa)	P (-)	φ ($^\circ$)	$\frac{D_{max}}{D_{min}}$	D_{50} (mm)
50	0.5	30	3	0.04

Table 1: Model parameters

266 The packing procedure used to generate the granular assembly involves
 267 the isotropic compression of an initial particles gas with the desired par-
 268 ticle size distribution. During this compression, the local contact friction
 269 angle is very low. The procedure outputs a sample with an isotropic fabric,
 270 a mean coordination number of 4.8 and a low porosity $n \approx 0.369$, under 1

271 kPa of isotropic pressure. On the other hand, the confining pressures con-
272 sidered here in the shearing phase range in the tens of kPa and the DEM
273 sample displays a typically dense behaviour [15].

274 3.2. *Hydraulic behaviour of the discrete model*

275 In the pursuit of fundamentals, the wetting and drying of a granu-
276 lar material is examined through DEM and provides a framework within
277 which we can verify the proposed stress equation derived from homoge-
278 nization.

279 Computing the water phase distribution, the discrete model allows us
280 to readily construct the Soil-Water Characteristic Curves (SWCC) numer-
281 ically. Hydraulic hysteresis is herein introduced through different liquid
282 bridge assumptions. As water vapour condensates primarily over solid
283 surfaces, initial wetting paths are simulated creating liquid bridges be-
284 tween contacting particles only. On the other hand, drying path simula-
285 tions involve liquid bridges between distant particles as well as contact-
286 ing particles, with the only condition being the existence of a solution to
287 Laplace's equation.

288 Fig. 3 depicts the drying and wetting SWCC of the discrete model to-
289 gether with some experimental data point for an Ottawa sand with a mean
290 diameter $D_{\text{mean}} \approx 0.172$ mm [27].

291 A limited hysteresis between drying and wetting is simulated because
292 known hysteresis mechanisms are not included in the numerical model.
293 First, the same contact angle value is considered upon drying and wetting.

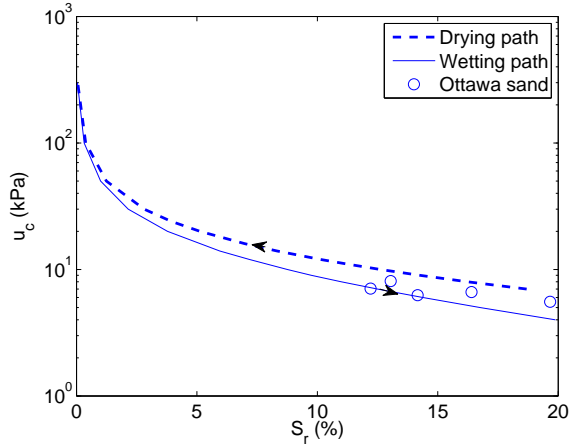


Figure 3: SWCCs of the discrete model. Ottawa sand data from [27]

294 Second, liquid bridges are uniformly distributed according to uniform ma-
 295 tric suction and particles distances and radii. As such, the control that
 296 smaller pores exert on the filling of larger pores according to the hydraulic
 297 loading path – the so-called ink-bottle effects – cannot be reproduced. Sim-
 298 ulation of such effects would certainly require the actual calculation of the
 299 flow of the two fluid phases inside the pore space, which is outside the
 300 scope of this paper.

301 4. Discussion of discrete modelling for multiphasic media

302 DEM may be considered as a numerical homogenization approach,
 303 where the stress tensor for a DEM sample arises from the interaction forces
 304 between discrete elements. However, when applied to multiphasic ma-
 305 terials, we argued in another work [16] that DEM provides an inconsis-
 306 tent average stress description, especially in the case where mechanical

307 actions corresponding to the fluid phases deviate significantly from be-
308 ing point forces. This inconsistency arises from the fact that actions of the
309 fluid phases on the solid phase are replaced by a resultant force, ignoring
310 the nature of their spatial distribution. Indeed, our volume-average stress
311 equation (12) reveals lineal forces due to surface tension and surface forces
312 due to fluid pressures, besides point forces at particle contacts. The above
313 important issue is next examined in greater details.

314 4.1. Biphasic case

315 For the fully saturated case involving a uniform water pressure u_w
316 within the pore space, replacing the action of liquid phase on the solid
317 phase with resultant forces would lead to the following within DEM cal-
318 culations:

- 319 • boundary DE (such as rigid platens) would sustain added forces
320 $\mathbf{f}^w = -u_w S \mathbf{n}$, with S the adequate surface and \mathbf{n} the inwards ex-
321 ternal normal,
- 322 • no extra forces would be imposed on any other DE since the water
323 phase induces no resultant forces on the solid phase in this case.

324 As such, total stresses defined from the resulting forces acting on bound-
325 ary DE are consistent with applied external loads. However, homogeniza-
326 tion of the forces interior to the discrete model towards these total stresses
327 is impossible, since the interior forces reflect the skeleton behaviour only,
328 corresponding to Terzaghi effective stress [11].

329 *4.2. Triphasic case*

330 As for the present unsaturated discrete model, the contact and capil-
331 lary forces interior to the model may be exactly homogenized to the total
332 stresses acting along the boundaries [39, 16], showing an additivity quali-
333 tatively similar to the one of the homogenization approach presented Sec-
334 tion 2.2. In the end, the total stress Σ for the unsaturated discrete model is
335 the sum of σ^{cont} , the same term as within the homogenization approach,
336 function of contact forces, and another stress tensor denoted again as a
337 capillary stress tensor $\sigma^{\text{cap}} = \Sigma - \sigma^{\text{cont}}$.

338 Within DEM, this capillary stress tensor is computed from the capil-
339 lary forces exerted by the fluid phases on the solid phase. However, fluid
340 phases are not simulated themselves, and point forces consideration does
341 not conform with both surface and lineal characters of the mechanical ac-
342 tions (fluid pressures and surface tension forces) exerted by the fluids on
343 the solid. For these reasons, the total stresses description of an unsaturated
344 soil as provided by the discrete model is not consistent with the averaging
345 approach of Section 2.2 in the general case. In fact, both approaches are
346 consistent when liquid volume and wetted surfaces as well as contours
347 tend to vanish, which is the case with a very good approximation for very
348 low degrees of saturation (few percents); otherwise substantial differences
349 appear [16].

350 To illustrate here this point, hydraulic loadings are imposed to the dis-
351 crete model. Wetting and drying paths are simulated by varying the ma-

352 tric suction under an isotropic stress state $p = 10$ kPa kept constant on the
 353 boundaries.

354 First, capillary stresses as described by the DEM, denoted $\sigma_{\text{DEM}}^{\text{cap}}$, are
 355 directly computed from capillary forces [39, 16]:

$$\sigma_{\text{DEM}}^{\text{cap}} = \frac{1}{V} \sum_l \mathbf{f}_\beta^{\text{cap}} \otimes \boldsymbol{\ell}_{\alpha\beta} \quad (16)$$

356 Equation (16) considers all particles pairs $\alpha\beta$ linked by a liquid bridge l ,
 357 with $\mathbf{f}_\beta^{\text{cap}}$ the capillary force as sustained by β , and $\boldsymbol{\ell}_{\alpha\beta}$ the so-called branch
 358 vector from the center of α to the center of β as defined earlier in the paper.

359 Second, we take advantage of the output the discrete model gives such
 360 as features of the liquid phase (filling angles α , menisci volumes) as it
 361 would exist in the simulated unsaturated soil. Hence, another capillary
 362 stress tensor $\sigma_{\text{hom}}^{\text{cap}}$ is computed using the homogenization formula (Eq.
 363 12):

$$\sigma_{\text{hom}}^{\text{cap}} = -s \boldsymbol{\chi} - \mathbf{B} \quad (17)$$

364 During hydraulic loading, both tensors $\sigma_{\text{DEM}}^{\text{cap}}$ and $\sigma_{\text{hom}}^{\text{cap}}$ turn out to
 365 be spherical (isotropic), with $\mathbf{B} = \mathbf{0}$ with regard to $\sigma_{\text{hom}}^{\text{cap}}$. Indeed, the
 366 packing of the DEM sample is here isotropic leading to an isotropic liq-
 367 uid bridge distribution, irrespective of whether a meniscus exists between
 368 contacting particles only (along the wetting path) or not (along the dry-
 369 ing path). Taking advantage of the sphericity of both capillary stress ten-
 370 sors in the above, the mean capillary pressures $p_{\text{DEM}}^{\text{cap}} = 1/3 \text{tr}(\sigma_{\text{DEM}}^{\text{cap}})$ and
 371 $p_{\text{hom}}^{\text{cap}} = 1/3 \text{tr}(\sigma_{\text{hom}}^{\text{cap}})$ are compared.

372 The discrepancies between $p_{\text{DEM}}^{\text{cap}}$ and $p_{\text{hom}}^{\text{cap}}$ mentioned earlier appear
 373 in Fig. 4. As in [16], the DEM model overestimates (in absolute value)
 374 the mean capillary pressure in the general case. For a common value at
 375 very low water contents ($S_r \rightarrow 0$), when both approaches are equivalent,
 376 $p_{\text{DEM}}^{\text{cap}}$ deviates more and more from $p_{\text{hom}}^{\text{cap}}$, up to 40-50% for $S_r = 15\%$.
 377 It is seen that this discrepancy increases according to the wetted surfaces
 378 which the discrete model does not directly take into account, contrary to
 379 the homogenization approach (Fig. 5). While qualitative trends are similar
 380 along wetting, influences of S_r on $p_{\text{DEM}}^{\text{cap}}$ and $p_{\text{hom}}^{\text{cap}}$ are even different along
 381 the drying path. This corresponds to greater wetted surfaces along drying
 382 rather than wetting (Fig. 5).

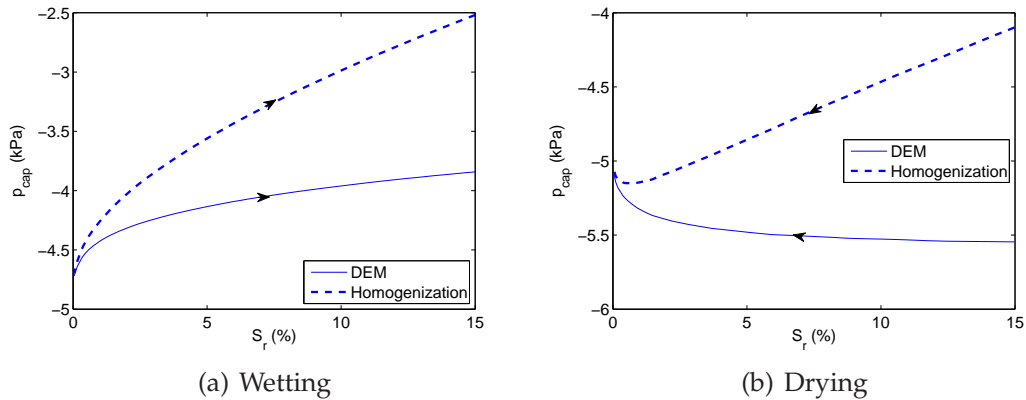


Figure 4: Capillary pressure from DEM or homogenization approach along hydraulic loadings (for both approaches p^{cap} is discontinuous at the origin, with $p^{\text{cap}}(S_r = 0) = 0$, not represented)

383 It is interesting to note that the higher wetted surfaces developed along
 384 the drying path than along the wetting path come from a higher number of

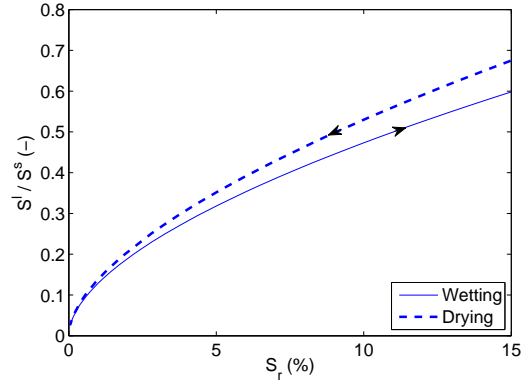


Figure 5: Solid surfaces wetted by the liquid, S^l , respective to whole solid surface S^s

385 liquid bridges. For a degree of saturation of 10% for instance, considering
 386 a drying path leads to 50% more liquid bridges between both distant and
 387 touching particles when compared with wetting. The average volume of
 388 these liquid bridges is consistently one third smaller, however each liquid
 389 bridge extends roughly along the same solid surface for both hydraulic
 390 loading paths. For these configurations, the average filling angle is 30.5°
 391 along drying, and 34.8° along wetting.

392 It is worth noticing that classical (“dry”) DEM simulations also encom-
 393 pass the current discussion of the validity of this method if actual physical
 394 forces are distributed. Indeed, the use of resultant forces is arguably pre-
 395 sented in [3] as adequate when contact areas (in reality), i.e. overlaps (in
 396 DEM models), are negligible—which is a classical assumption for the va-
 397 lidity of DEM [14, 34, 37, 22]. As for the homogenization approach, this
 398 assumption enters directly into the computations, so that $\int \sigma \mathbf{n} \otimes \mathbf{x} dS$ can
 399 be replaced by $\sum \mathbf{f} \otimes \mathbf{x}$ [2].

400 Finally, we wish to conclude from these results that DEM applied to
401 multiphasic materials provides in some cases an inconsistent description
402 of the average, or total, stresses. Obviously, such description is in fact
403 not relevant for saturated cases for which the behaviour is known to be
404 governed by Terzaghi's effective stress, provided that both fluid and solid
405 phases are incompressible. However, it is in our opinion that searching for
406 a single-valued effective stress for the unsaturated case through numerical
407 experiments, total stresses have first to be adequately simulated.

408 5. Hydraulic loading

409 We focus now on the capillary stress tensor, as computed from the ho-
410 mogenization approach. First, we consider the same hydraulic loading
411 paths as in Section 4.2. Regarding the discussion on the comparison be-
412 tween DEM and the homogenization approach, only wetting paths are
413 considered, up to a maximum degree of saturation $S_r = 10\%$, so that
414 DEM and the homogenization approach are consistent, qualitatively and
415 to some extent quantitatively.

416 5.1. Isotropic packings

417 The initial isotropic packing of the sample confers an isotropy to the
418 liquid phase, given that liquid bridges appear at every geometrical con-
419 tacts. As mentioned earlier, this makes the capillary stress tensor to be
420 spherical, with $\sigma^{\text{cap}} = -s\chi$ since $\mathbf{B} = \mathbf{0}$ for isotropic packings, under a
421 zero contact angle assumption.

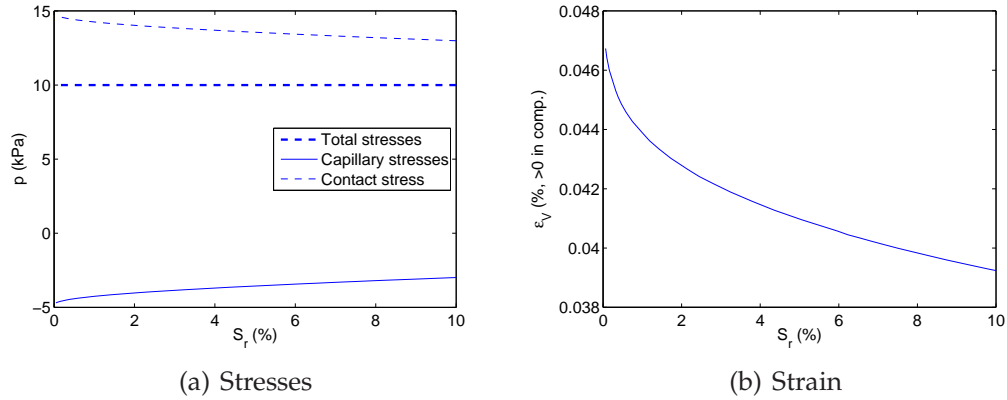


Figure 6: Wetting of an isotropic sample

422 A significant capillary stress ($p_{\text{cap}} \approx -5$ kPa for $S_r \rightarrow 0$) is developed at
 423 the drying-wetting transition (Fig. 6(a)). Further wetting makes the capil-
 424 lary stress decrease (in absolute value) because of the decrease in suction
 425 that is not counterbalanced by the increase in wetted surfaces upon which
 426 χ depends. As for the strains, pure volumetric strains are induced dur-
 427 ing wetting of the isotropic sample. The drying-wetting transition causes
 428 the sample to contract due to the development of attractive internal forces.
 429 The volumetric response is thereafter dilatant upon further wetting (Fig.
 430 6(b)), because at the meniscus scale liquid bonding decreases in intensity
 431 when suction decreases for menisci between contacting particles [16].

432 This behaviour is qualitatively consistent with the trends of $p_{\text{cont}} =$
 433 $p - p_{\text{cap}}$ (Fig. 6(a)), if an elastic behaviour were assumed between strains
 434 and the particle contact stress $\sigma^{\text{cont}} = \sigma - \sigma^{\text{cap}}$. For later reference, Section
 435 7 investigates more carefully whether this stress tensor can be regarded as

436 an effective stress or not.

437 5.2. *Induced anisotropic packings*

438 Non-isotropic packings are now considered, for the induced anisotropy
 439 case. An initially isotropic DEM sample is compressed along the vertical
 440 direction under dry triaxial (axisymmetric) conditions with a confining
 441 pressure $\sigma_{\text{lat}} = 10$ kPa. Axial compressions up to 0.1, 0.2 and 0.3% define
 442 three states A, B and C as given in Table 2 and Fig. 7.

Designation	Axial strain after the initial dry compression (%)	$\eta = q/p$ (-)
State A	0.1	0.85
State B	0.2	1.03
State C	0.3	1.06

Table 2: Anisotropic states

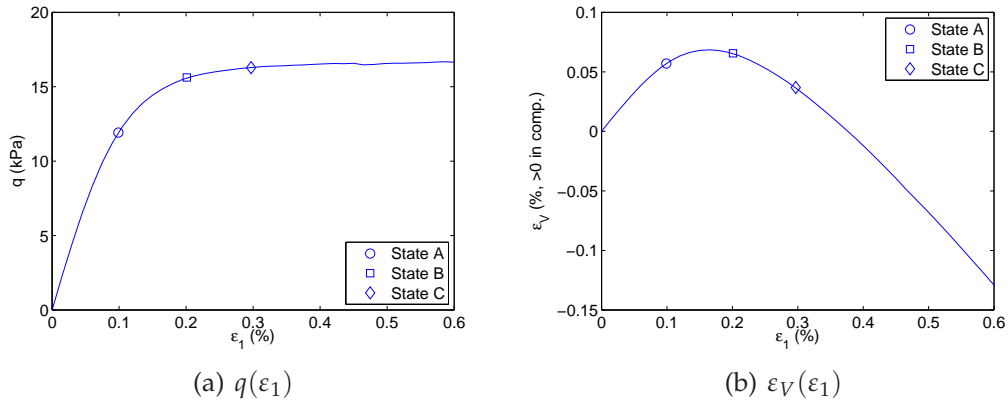


Figure 7: Initial dry axisymmetric compression defining States A, B and C

443 After an axial strain of 0.1%, plastic deformations with particle rear-
 444 rangement has not yet fully developed; thus State A is almost isotropic

445 (Fig. 8(a)). On the other hand, States B and C are close to the peak stress,
 446 and thus induced anisotropy appears clearly in Fig. 8(b) and 8(c), with the
 447 State C being more marked due to a greater plastic deformation. However,
 differences in SWCC are negligible between the three states (Fig 9).

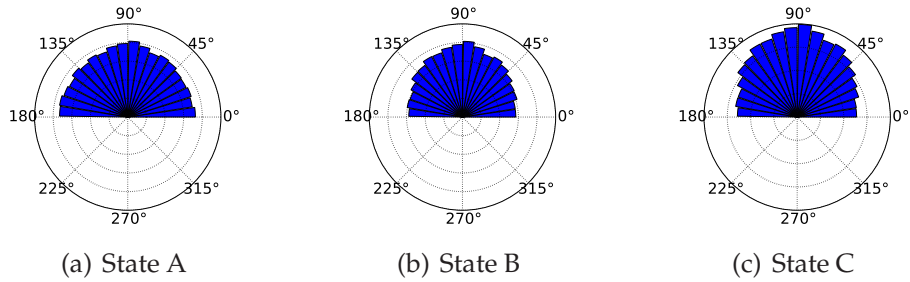


Figure 8: Contact directions in a plane of symmetry (y -direction corresponds to 90°)

448

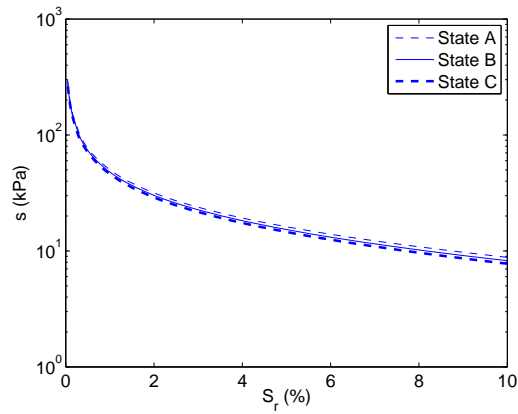


Figure 9: SWCC for the anisotropic states

449 Although wetting is being imposed to the three different states under
 450 a constant total stress, a deviatoric component for the capillary stresses in-
 451 terestingly appears due to the induced anisotropy (Fig. 10(b)). As such,
 452 the deviatoric capillary stress increases (in absolute value) from State A to

453 State C, irrespective of the water content. Except for the dry-wet transition,
 454 variations in water content have generally little effect on the deviatoric
 455 capillary stress. Indeed, an increasing degree of saturation reduces the de-
 456 viatoric component of $-s\chi$ on one hand, and increases that of $-B$ on the
 457 other hand (Fig. 11). An increase in the deviatoric component of $-B$ (i.e.
 458 its norm) upon saturation corresponds to greater menisci contours along
 459 which surface tension forces act. On the other hand, the decrease in suc-
 460 tion associated with saturation is responsible for decreasing the deviatoric
 461 part and the mean pressure (Fig. 10(a)) of $-s\chi$. Considering the differ-
 462 ent states, the mean capillary stress is observed to decrease (in absolute
 463 value) from State A to State C. This comes from a decreasing coordination
 464 number between State A and C, creating here less liquid bridges.

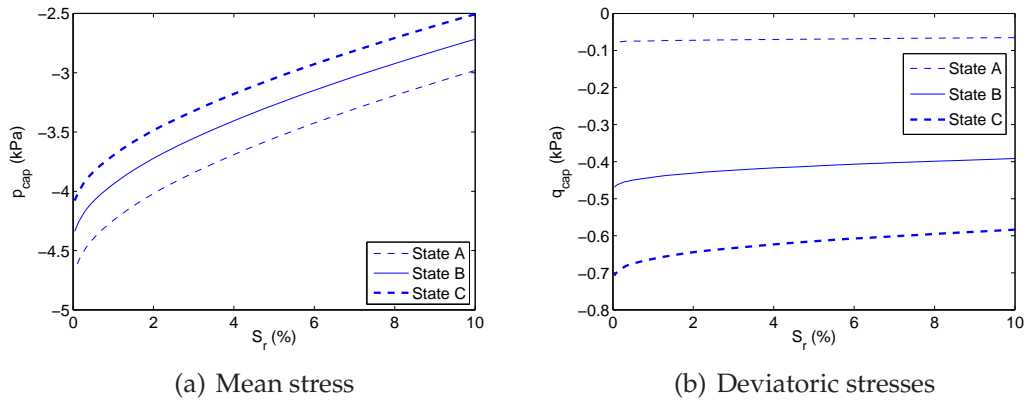


Figure 10: Capillary stresses during wetting of anisotropic packings

465 As for the strains, the wetting of anisotropic assemblies clearly induces
 466 deviatoric strains, in addition to the volumetric ones. The deviatoric strain

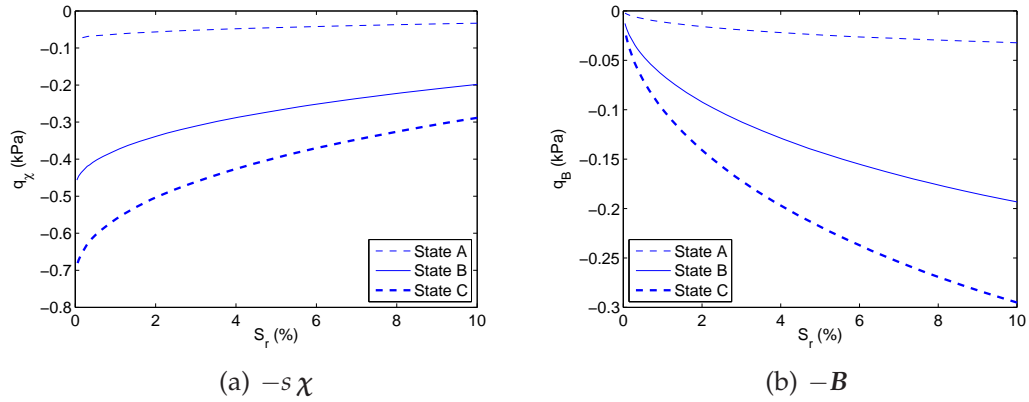


Figure 11: Deviatoric components of the two parts of the capillary stress tensor

467 appears at the dry-unsaturated transition, and can be considered as con-
 468 stant upon further wetting (Fig. 12(b)). The deviatoric strain values are
 469 greater from State A to State C. As for the volumetric strains, they show the
 470 same trends upon wetting as for the previous isotropic packing (Fig. 12(a)
 471 and 6(b)). For a given water content, the volumetric strains are reduced
 from State A to State C.

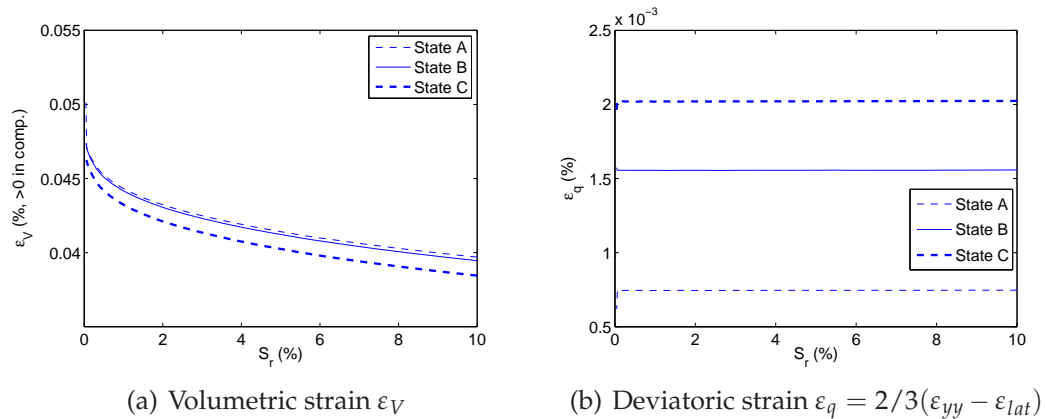


Figure 12: Deformations (with respect to the dry states A, B or C) upon wetting of anisotropic packings

472

473 Both volumetric and deviatoric strain changes are qualitatively consis-
 474 tent with the changes of the intra-granular stress $\sigma^{\text{cont}} = \Sigma - \sigma^{\text{cap}}$ (Fig. 13)
 475 but these results do show yet any quantitative comparison.

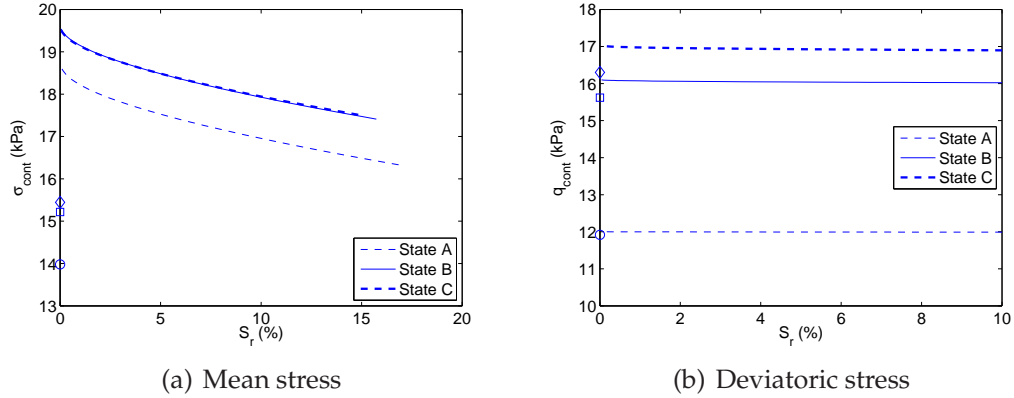


Figure 13: Intra-granular stress $\sigma^{\text{cont}} = \sigma - \sigma^{\text{cap}}$ upon wetting of anisotropic packings. Symbols correspond to σ^{cont} in the dry case, after the initial dry compression. They correspond also to the constant total stresses during wetting

476 6. Mechanical loading and anisotropy of the capillary stress tensor

477 The capillary stress tensor $\sigma_{\text{hom}}^{\text{cap}} = -(s\chi + B)$ is now computed us-
 478 ing Eq. (12) along triaxial and simple shear loadings (see Fig. 14). The
 479 loading paths are applied to the discrete model for low degrees of sat-
 480 uration (Table 3), so that both approaches are quantitatively consistent:
 481 $\sigma_{\text{hom}}^{\text{cap}} \approx \sigma_{\text{DEM}}^{\text{cap}} \approx \sigma^{\text{cap}}$. Considering initial states resulting from a wetting
 482 path, menisci are created at geometrical contacts only. Hence, initial states
 483 show in average five menisci per particle. Then, menisci are kept when
 484 initially touching particles separate during loading, as long as Laplace's
 485 equation can be solved. Note that triaxial simulations involve frictionless

486 rigid platens as boundary DE, while simple shear simulations use periodic
 487 boundaries. The periodic sample used for simple shear simulations is as
 488 close as possible to the non-periodic one used for triaxial simulations, see
 489 [15].

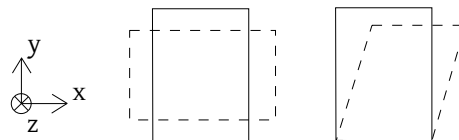


Figure 14: Triaxial loading (left): $\Sigma_I = \Sigma_{yy} > \Sigma_{II} = \Sigma_{xx} = \Sigma_{III} = \Sigma_{zz} = \Sigma_{lat} = cst$, and simple shear loading (right): $\partial v_x / \partial y = cst$, $\Sigma_{yy} = \Sigma_{zz} = \Sigma_{lat} = cst$

Table 3: Considered mechanical loading paths

Loading type	Σ_{lat} (kPa)	s (kPa)	Initial S_r (%)
Triaxial	10	20	3.78
"	"	50	1.00
"	"	100	0.32
"	"	300	0.05
Simple shear	"	50	1.16
"	"	300	0.05

490 We focus on the relative contributions of the terms $s\chi$ and \mathbf{B} , and
 491 the anisotropy (deviatoric nature) of the capillary stress. Tensors are rep-
 492 resented using three invariants: the mean stress p , the deviatoric stress
 493 $q = \Sigma_{yy} - \Sigma_{lat}$ (for triaxial loadings) or $|q| = \sqrt{3/2} \|s\| = \sqrt{3/2} \|\Sigma - p\delta\|$
 494 (for simple shears), and the Lode angle $\theta = 1/3 \arccos(27/2 \det(s)/|q|^3)$.
 495 For instance, $\theta = 0^\circ$ for triaxial compression.

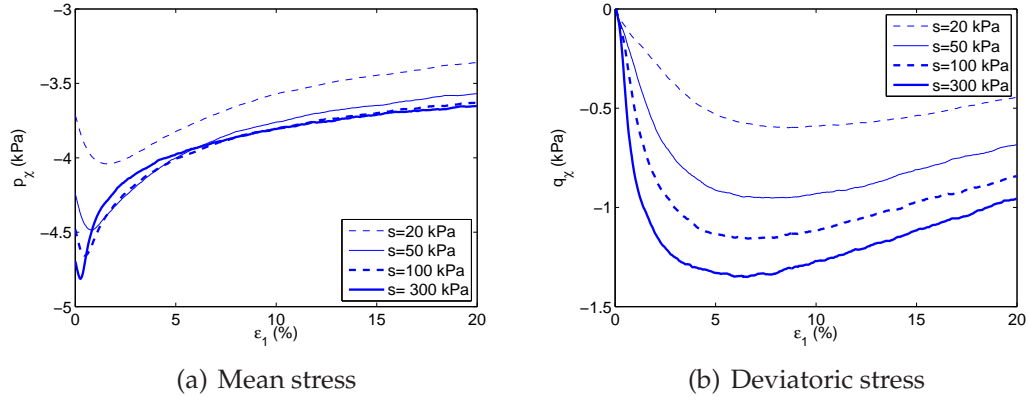


Figure 15: Invariants of $-s\chi$ for triaxial loadings with different suctions

496 As explained earlier, the initially isotropic packing makes the capillary
 497 stress to be spherical and equal to $-s\chi$ ($\mathbf{B} = \mathbf{0}$) at the start of the
 498 triaxial loading (Fig. 15 and 16). As the loading progresses and induced
 499 anisotropy develops, the deviatoric nature of the capillary stress tensor, as
 500 measured by $|q_{\text{cap}}|/p_{\text{cap}}$, rapidly builds up (Fig. 17). For low suctions this
 501 deviatoric nature arises from the tensor $-\mathbf{B}$ describing the spatial distri-
 502 bution of surface tension forces, whereas for high suctions it is the spa-
 503 tial distribution of matric suction ($-s\chi$) term that governs. Indeed, for a
 504 given strain value, Fig. 15(b) and 16 confirm the influence of matric suc-
 505 tion shown previously: the deviatoric part of ($-s\chi$) increases according
 506 to suction, due to the proportionality with s , whereas the deviatoric tensor
 507 \mathbf{B} decreases in norm with suction because of dwindling wetted contours.

508 Changes in the mean and deviatoric parts of the capillary stress with
 509 suction follow the same trends for simple shear loading [15]. Furthermore,

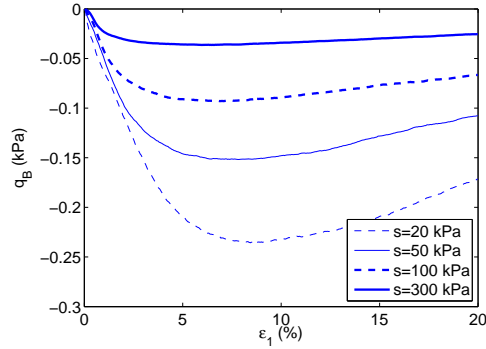


Figure 16: Deviatoric stress of $-B$ for triaxial loadings with different suctions

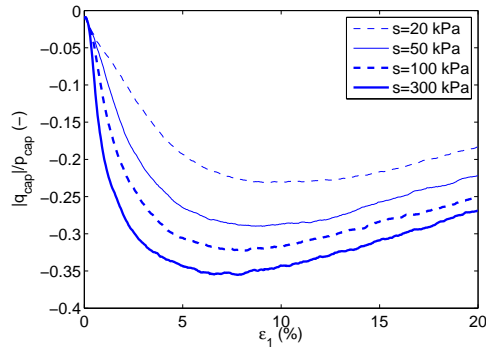


Figure 17: Deviatoric feature of $\sigma^{cap} = -s\chi - B$ for triaxial loadings with different suctions

510 the mechanical actions described by tensors $-s\chi$ and $-B$ present the same
 511 Lode angles in simple shear (Fig. 18).

512 7. Effective stress

513 We finally focus our attention to the particle contact stress σ^{cont} which
 514 is essentially an intra-granular stress for very low saturation ratios $S_r <$
 515 1% for which DEM is equivalent to the homogenization approach. The
 516 DEM model is used to impose various total stresses Σ and compute the

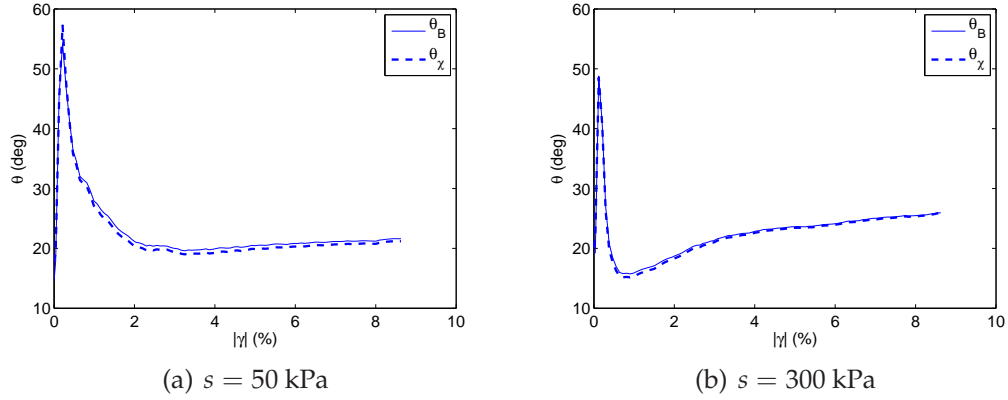


Figure 18: Lode angles of the two parts of the capillary stress tensor for simple shears

517 capillary stress $\sigma^{\text{cap}} = -s \chi - B$. The intra-granular stress is finally indi-
 518 rectly deduced from $\sigma^{\text{cont}} = \Sigma - \sigma^{\text{cap}}$.

519 *7.1. Constitutive relevancy of the intra-granular stress*

520 First, two triaxial loadings in dry and wet conditions are considered.
 521 A confining pressure close to 25 kPa is applied in the dry test, whereas 20
 522 kPa of confining pressure together with 300 kPa of suction are imposed in
 523 the unsaturated case. This corresponds throughout the wet test to a de-
 524 gree of saturation $S_r \approx 0.04\% \pm 0.01\%$. The intra-granular stresses σ^{cont}
 525 cannot be directly controlled during wet simulations and these loading
 526 parameters allow σ^{cont} to be as close as possible during both simulations,
 527 see Fig. 19(a). It turns out that a significant discrepancy appears on the
 528 resulting strain paths as seen in Fig. 19(b). In fact, the stress tensor σ^{cont}
 529 can arguably be considered as specific to the solid phase since it describes
 530 the stresses arising inside the solid grains due to other solid grains. How-

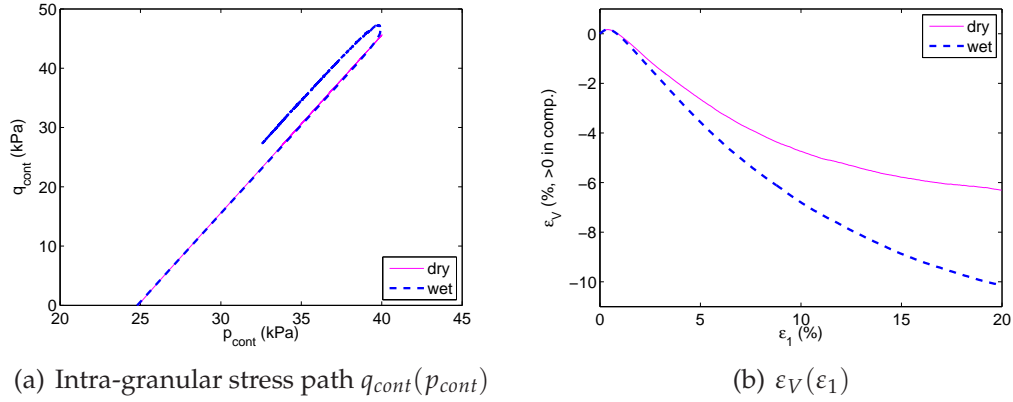


Figure 19: Comparable loading paths in dry and wet conditions

531 ever, as illustrated by our results, the straining of the solid phase inside
 532 the unsaturated REV (i.e. straining of the unsaturated REV itself) is af-
 533 fected by the behaviour of the other phases and also the coupling between
 534 the different phases [30]. For that reason, we observe different behaviours
 535 between the dry and wet cases.

536 It is probable that the observed strains of the unsaturated REV could
 537 still be interpreted using σ^{cont} as a stress variable, through a phenomeno-
 538 logical elasto-plastic approach including suction hardening [10].

539 7.2. A unique plastic limit criterion

540 In this last section, attention is paid to the attainment of limit plastic
 541 stress states starting from several triaxial and simple shear loading paths
 542 under both dry and wet conditions. Confining pressures range between 5
 543 and 25 kPa and, for the unsaturated cases, suction values from 50 to 600
 544 kPa; which corresponds to different degrees of saturation below 1%. The

545 limit stress states are defined as the maxima of $(q f(\theta)/p)$, with the Lode
 546 angle influence $f(\theta)$ is assumed to obey Lade criterion [24].

547 Whereas no unique plastic limit criterion appears for the total stresses
 548 in both dry and wet conditions as seen in Fig. 20(a), the use of σ^{cont} makes
 549 all data points fit within an acceptable agreement into a unique plastic
 550 limit criterion corresponding (for triaxial compression) to a Mohr-Coulomb
 551 friction angle $\phi_{MC} \approx 29^\circ$ (Fig. 20(b)). This suggests that the intra-granular
 552 stress defined as $\sigma^{\text{cont}} = \Sigma - \sigma^{\text{cap}}$ is the adequate variable to express the
 strength of the DEM assembly in both dry and wet conditions.

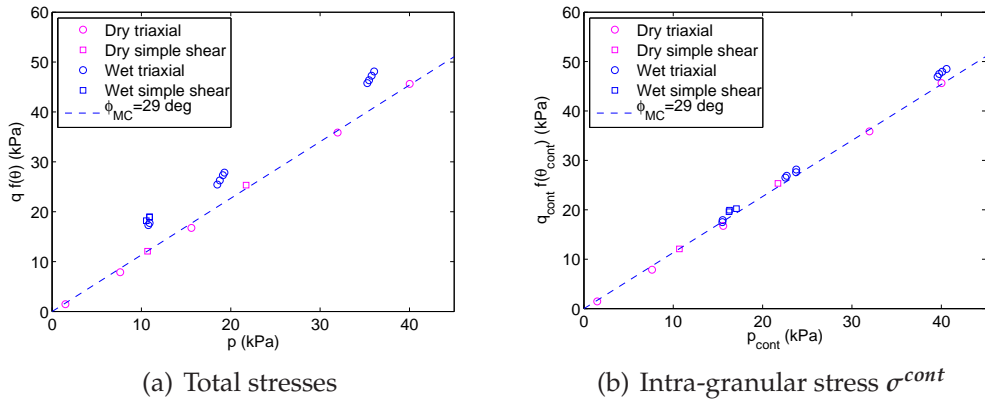


Figure 20: Plastic limit criterion for the granular soil in dry and wet conditions

553

554 8. Conclusion

555 The microscopic stresses within an unsaturated pendular granular soil
 556 have been volume-averaged to give a tensorial form for the macroscopic
 557 stress. The averaging process considers in particular interfacial stress tensors
 558 specific for the discontinuity surfaces between air and water. Deriva-

559 tions led to the expression of the total net stress tensor as the sum of a cap-
560 illary stress tensor, describing mechanical actions pertaining to the liquid
561 bridges and interface surfaces, and a contact stress tensor, encompassing
562 the contact forces between solid grains.

563 These different stress tensors have been evaluated and verified using a
564 DEM model for unsaturated granular soils. A major finding is that com-
565 parisons between the DEM and the homogenization approach is strictly
566 speaking valid only for very low degrees of saturation, at the low end of
567 the pendular regime. For higher water content, internal forces such as wa-
568 ter pressure and surface tension forces act on finite surfaces, whereas DEM
569 can only consider resultant point forces, which leads to an inconsistent de-
570 scription of total stresses for the unsaturated REV.

571 Using then the DEM model in conjunction with the averaging proce-
572 dure for very low water content, the capillary stresses have been shown
573 to be anisotropic in the general case. Non-spherical stress tensors are thus
574 required to describe these capillary stresses, in contradiction with the clas-
575 sical Bishop's equation and current modelling approaches.

576 Furthermore, the effective nature of the particle contact stress tensor
577 has been discussed. From a theoretical standpoint, this stress tensor can-
578 not be used to assess deformations in an unsaturated sample in the same
579 manner as for a dry one. However, results from triaxial and simple shear
580 loading paths point to show the particle contact stress tensor does unify
581 the description of failure in unsaturated and dry granular soils. Further

582 investigations of homogenization approaches wherein strains are also in-
 583 troduced along with the consideration of interfaces and compressibility of
 584 phases should provide further answers to open questions as to the exis-
 585 tence of a single-valued stress tensor that controls deformations in unsat-
 586 urated granular assemblies.

587 Acknowledgements

588 This work is supported by the Natural Science and Engineering Re-
 589 search Council of Canada and Foundation Computer Modelling Group
 590 within the framework of a Government-Industry Partnership (NSERC-
 591 CRD) Grant towards the fundamental understanding of complex multi-
 592 phasic granular media.

593 Appendix A.

594 Recall Stokes's theorem:

$$\int_C \mathbf{F} \cdot d\boldsymbol{\ell} = \int_S \mathbf{n} \cdot (\nabla \times \mathbf{F}) dS \quad (\text{A.1})$$

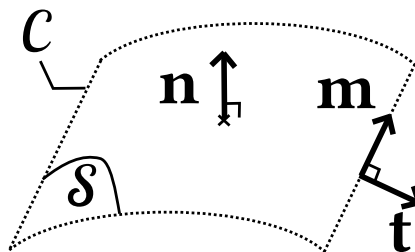


Figure A.1: Definition of surface S , contour C and associated vectors

595 Let $\mathbf{F} = \mathbf{f} \times \mathbf{b}$ and $d\ell = \mathbf{m} d\ell$ where \mathbf{b} is a constant vector and \mathbf{m} the
 596 unit vector tangent to contour \mathcal{C} . Then,

$$\int_{\mathcal{C}} (\mathbf{f} \times \mathbf{b}) \cdot \mathbf{m} d\ell = \int_S \mathbf{n} \cdot (\nabla \times (\mathbf{f} \times \mathbf{b})) dS \quad (\text{A.2})$$

597 Using identities

$$\begin{aligned} (\mathbf{f} \times \mathbf{b}) \cdot \mathbf{m} &= -\mathbf{b} \cdot (\mathbf{f} \times \mathbf{m}) \\ \nabla \times (\mathbf{f} \times \mathbf{b}) &= -\mathbf{b}(\nabla \cdot \mathbf{f}) + \mathbf{b} \cdot \nabla \mathbf{f} \end{aligned} \quad (\text{A.3})$$

598 and since \mathbf{b} is an arbitrary vector,

$$\int_{\mathcal{C}} (\mathbf{f} \times \mathbf{m}) d\ell = \int_S \mathbf{n}(\nabla \cdot \mathbf{f}) - (\nabla \mathbf{f}) \cdot \mathbf{n} dS \quad (\text{A.4})$$

599 If we choose $\mathbf{f} = \gamma \mathbf{n}$ and recalling that $\mathbf{n} \times \mathbf{m} = -\mathbf{t}$

$$\begin{aligned} -\int_{\mathcal{C}} \gamma \mathbf{t} d\ell &= \int_S \mathbf{n}(\nabla \cdot (\gamma \mathbf{n}) - (\nabla \gamma \mathbf{n}) \cdot \mathbf{n}) dS \\ &= \int_S [\mathbf{n} \nabla \gamma \cdot \mathbf{n} + \gamma \mathbf{n}(\nabla \cdot \mathbf{n}) - \nabla \gamma - \gamma(\nabla \mathbf{n}) \cdot \mathbf{n}] dS \end{aligned} \quad (\text{A.5})$$

600 Since $\nabla \gamma$ is tangent to surface S and $(\nabla \mathbf{n}) \cdot \mathbf{n} = \frac{1}{2} \nabla(\mathbf{n} \cdot \mathbf{n}) = \frac{1}{2} \nabla(1) = 0$,
 601 we finally get:

$$\int_{\mathcal{C}} \gamma \mathbf{t} d\ell = \int_S [\nabla \gamma - \gamma \mathbf{n}(\nabla \cdot \mathbf{n})] dS \quad (\text{A.6})$$

602 References

603 References

604 [1] Alonso, E. E., Gens, A., Josa, A., 1990. A constitutive model for
 605 partially saturated soils. *Géotechnique* 40, 405–430(25).

606 URL <http://www.icevirtuallibrary.com/content/article/10.1680/geot.1990.40.3.4>

607 [2] Bagi, K., 1996. Stress and strain in granular assemblies. *Mechanics of*
608 *Materials* 22 (3), 165 – 177.

609 [3] Bathrust, R. J., Rothenburg, L., 1990. Observations on stress-force-
610 fabric relationships in idealized granular materials. *J. Mechanics of*
611 *materials* 9, 65–80.

612 [4] Biarez, J., Fleureau, J., Taibi, S., 1993. Constitutive model for unsat-
613 urated granular media made up by spheres. In: Thornton, C. (Ed.),
614 Proc. 2nd Int. Conference on Micromechanics of Granular Media.
615 Balkema, Birmingham, UK, pp. 51–58.

616 [5] Bishop, A., 1959. The principle of effective stress. *Teknisk Ukeblad* 39,
617 859–863.

618 [6] Bishop, A. W., Blight, G. E., 1963. Some aspects of effective stress in
619 saturated and partly saturated soils. *Géotechnique* 13, 177–197.

620 [7] Blight, G., 1965. A study of effective stress for volume change. In:
621 Aitchison, G. (Ed.), *Moisture Equilibria and Moisture Changes in*
622 *Soils beneath Covered Areas*. Butterworths, pp. 259–269.

623 [8] Bluhm, J., de Boer, R., 1996. Effective stresses – a clarification. *Archive*
624 *of Applied Mechanics* 66 (7), 479–492.

625 URL <http://dx.doi.org/10.1007/BF00790180>

- 626 [9] Borja, R. I., 2004. Cam-clay plasticity. part v: A mathematical frame-
627 work for three-phase deformation and strain localization analyses
628 of partially saturated porous media. *Computer Methods in Applied
629 Mechanics and Engineering* 193 (48-51), 5301 – 5338, advances in
630 Computational Plasticity.
631 URL <http://www.sciencedirect.com/science/article/pii/S0045782504002762>
- 632 [10] Borja, R. I., 2006. On the mechanical energy and effective stress in
633 saturated and unsaturated porous continua. *International Journal of
634 Solids and Structures* 43 (6), 1764 – 1786.
- 635 [11] Catalano, E., Chareyre, B., Barthélémy, E., 2014. Pore-scale modeling
636 of fluid-particles interaction and emerging poromechanical effects.
637 *International Journal for Numerical and Analytical Methods in Ge-
638 omechanics* 38 (1), 51–71.
- 639 [12] Chareyre, B., Cortis, A., Catalano, E., Barthélemy, E., 2012. Pore-scale
640 modeling of viscous flow and induced forces in dense sphere pack-
641 ings. *Transport in Porous Media* 94 (2), 595–615.
- 642 [13] Chateau, X., Dormieux, L., 2002. Micromechanics of saturated and
643 unsaturated porous media. *International Journal for Numerical and
644 Analytical Methods in Geomechanics* 26 (8), 831–844.
- 645 [14] Cundall, P., Strack, O., 1979. A discrete numerical model for granular
646 assemblies. *Géotechnique* 29, 47–65.

- 647 [15] Duriez, J., Wan, R., 2015a. Effective stress in unsaturated granular ma-
648 terials: micro-mechanical insights. In: Coupled Problems in Science
649 and Engineering VI. pp. 1232–1242.
- 650 [16] Duriez, J., Wan, R., 2015b. Micromechanics of wet granular soils and
651 issues in discrete element modelling. *Géotechnique* – under review.
- 652 [17] Fredlund, D., Morgenstern, N., 1977. Stress state variables for unsatu-
653 rated soils. *Journal of Geotechnical and Geoenvironmental Engineer-*
654 *ing* 103 (GT5), 447–466.
- 655 [18] Gray, W. G., Hassanizadeh, S. M., 1991. Unsaturated flow theory
656 including interfacial phenomena. *Water Resources Research* 27 (8),
657 1855–1863.
- 658 [19] Gray, W. G., Schrefler, B. A., Pesavento, F., 2009. The solid phase stress
659 tensor in porous media mechanics and the hill-mandel condition.
660 *Journal of the Mechanics and Physics of Solids* 57 (3), 539 – 554.
661 URL <http://www.sciencedirect.com/science/article/pii/S0022509608001968>
- 662 [20] Hassanizadeh, S., Gray, W. G., 1990. Mechanics and thermodynamics
663 of multiphase flow in porous media including interphase bound-
664 aries. *Advances in Water Resources* 13 (4), 169 – 186.
665 URL <http://www.sciencedirect.com/science/article/pii/030917089090040B>
- 666 [21] Houlsby, G. T., 1997. The work input to an unsaturated granular

- 667 material. *Géotechnique* 47, 193–196(3).
668 URL <http://www.icevirtuallibrary.com/content/article/10.1680/geot.1997.47.1.1>
- 669 [22] Huang, X., O’Sullivan, C., Hanley, K., Kwok, C., 2014. Discrete-
670 element method analysis of the state parameter. *Géotechnique* 64,
671 954–965(11).
- 672 [23] Jennings, J. E. B., Burland, J. B., 1962. Limitations to the use of effec-
673 tive stresses in partly saturated soils. *Géotechnique* 12, 125–144(19).
674 URL <http://www.icevirtuallibrary.com/content/article/10.1680/geot.1962.12.2.1>
- 675 [24] Lade, P. V., Duncan, J. M., 1975. Elasto-plastic stress-strain theory for
676 cohesionless soil. *Journal of the Geotechnical Engineering Division*
677 101 (10), 1037–1053.
- 678 [25] Laplace, P. S., 1806. Sur l’action capillaire in *Supplément au Livre X*
679 *du Traité de Mécanique Céleste*. Duprat (Paris), available in *Oeuvres*
680 *complètes de Laplace, Tome 4*, on www.gallica.bnf.fr.
- 681 [26] Li, X., 2003. Effective stress in unsaturated soils: a microstructural
682 analysis. *Géotechnique* 53 (2), 273–277.
- 683 [27] Likos, W. J., 2014. Effective stress in unsaturated soil: Accounting for
684 surface tension and interfacial area. *Vadose Zone Journal* 13 (5), 1–12.
- 685 [28] Love, A., 1927. *A treatise on the mathematical theory of elasticity*.
686 Cambridge University Press, Cambridge.

- 687 [29] Lu, L., Likos, W., 2004. *Unsaturated Soil Mechanics*. John Wiley.
- 688 [30] Madeo, A., dell'Isola, F., Darve, F., 2013. A continuum model for
689 deformable, second gradient porous media partially saturated with
690 compressible fluids. *Journal of the Mechanics and Physics of Solids*
691 61 (11), 2196 – 2211.
692 URL <http://www.sciencedirect.com/science/article/pii/S002250961300121X>
- 693 [31] Mani, R., Kadau, D., Herrmann, H. J., 2013. Liquid migration in
694 sheared unsaturated granular media. *Granular Matter* 15 (4), 447–454.
- 695 [32] Nuth, M., Laloui, L., 2008. Effective stress concept in unsaturated
696 soils: Clarification and validation of a unified framework. *International Journal for Numerical and Analytical Methods in Geomechanics*
697 32 (7), 771–801.
698
- 699 [33] Pietruszczak, S., Pande, G., 1991. On the mechanics of partially satu-
700 rated soils. *Computers and Geotechnics* 12 (1), 55–71.
- 701 [34] Potyondy, D., Cundall, P., 2004. A bonded-particle model for rock.
702 *International Journal of Rock Mechanics and Mining Sciences* 41 (8),
703 1329 – 1364.
- 704 [35] Richefeu, V., E. Y. M. S., Radjai, F., 2006. Shear strength properties of
705 wet granular materials. *Phys. Rev. E* 73, 051304–1 –051304–11.
- 706 [36] Rosenkilde, C. E., 1967. Surface-energy tensors. *Journal of Mathematical Physics*
707 8 (1).

- 708 [37] Roux, J.-N., Chevoir, F., 2005. Discrete numerical simulation and the
709 mechanical behavior of granular materials. *Bulletin des laboratoires*
710 *des ponts et chaussées* 254, 109–138.
- 711 [38] Scholtès, L., Chareyre, B., Nicot, F., Darve, F., 2009. Micromechanics
712 of granular materials with capillary effects. *International Journal of*
713 *Engineering Science* 47 (1), 64 – 75.
- 714 [39] Scholtès, L., Hicher, P.-Y., Nicot, F., Chareyre, B., Darve, F., 2009.
715 On the capillary stress tensor in wet granular materials. *International*
716 *Journal for Numerical and Analytical Methods in Geomechanics*
717 33 (10), 1289–1313.
- 718 [40] Schrefler, B., 1995. F.e. in environmental engineering: Coupled
719 thermo-hydro-mechanical processes in porous media including pol-
720 lutant transport. *Archives of Computational Methods in Engineering*
721 2 (3), 1–54.
722 URL <http://dx.doi.org/10.1007/BF02736173>
- 723 [41] Skempton, A., 1961. Effective stress in soils, concrete and rock. In: In:
724 *Pore Pressure and Suction in Soils*. Butterworth, pp. 4–16.
- 725 [42] Vlahinić, I., M.J., H., Andrade, J., Thomas, J., 2011. A novel and gen-
726 eral form of effective stress in a partially saturated porous material:
727 The influence of microstructure. *Mechanics of Materials* 43 (1), 25 –

- 728 35.
729 URL <http://www.sciencedirect.com/science/article/pii/S0167663610001547>
- 730 [43] Šmilauer, V., Catalano, E., Chareyre, B., Dorofeenko, S., Duriez, J.,
731 Gladky, A., Kozicki, J., Modenese, C., Scholtès, L., Sibille, L., Strán-
732 ský, J., Thoeni, K., 2010. Yade Documentation, 1st Edition. The Yade
733 Project, <http://yade-dem.org>.
- 734 [44] Wan, R., Khosravani, S., Pouragha, M., 2014. Micromechanical analy-
735 sis of force transport in wet granular soils. *Vadose Zone Journal* 13 (5).
736 URL <http://vzj.geoscienceworld.org/content/13/5/vzj2013.06.0113.abstract>
- 737 [45] Weber, J., 1966. Recherches concernant les contraintes intergranu-
738 laires dans les milieux pulvérulents. *Bulletin de liaison des Ponts et*
739 *Chaussées* 20, 1–20.